ELSEVIER

Wear 252 (2002) 946–955

WEAR

www.elsevier.com/locate/wear

# Wear stability of polymer nanocomposite coatings with trilayer architecture

A. Sidorenko [a], Hyo-Sok Ahn [b], Doo-In Kim [b], H. Yang [a], V.V. Tsukruk [a,*]

[a] *Department of Materials Science and Engineering, Iowa State University, 3155 Gilman Hall, Ames, IA 50011, USA*
[b] *Tribology Research Center, Korea Institute of Science and Technology, 39-1 Hawolgok-dong, Songbuk-gu, Seoul 136-791, South Korea*

Received 2 November 2001; received in revised form 12 March 2002; accepted 12 March 2002

**Abstract**

A polymer trilayer (sandwiched) film with a thickness of 20–30 nm has been designed to serve as a wear resistant nanoscale coating for silicon surfaces. These surface structures are formed by a multiple grafting technique applied to self-assembled monolayers (SAM) and functionalized tri-block copolymer, followed by the photopolymerization of a topmost polymer layer. The unique design of this layer includes a hard-soft-hard nanoscale architecture with a compliant rubber interlayer mediating localized stresses transferred through the topmost hard layer. This architecture provides a non-linear mechanical response under a normal compression stress and allows additional dissipation of mechanical energy via the highly elastic rubber interlayer. At modest loads, this coating shows friction coefficient against hard steel below 0.06, which is lower than that for a classic molecular lubricant, alkylsilane SAM. At the highest pressure tested in this work, 1.2 GPa, the sandwiched coating possesses four times higher wear resistance than the SAM coating. The wear mechanism for this coating is stress and temperature induced oxidation in the contact area followed by severe plowing wear. © 2002 Elsevier Science B.V. All rights reserved.

*Keywords:* Wear stability; MEMS; Nanocomposite coatings; Boundary lubricants

## 1. Introduction

The development of silicon-based micro-device technology has initiated interest in sophisticated coatings with a nanoscale thickness. The nano-mechanical behavior of such coatings plays an important role in the reliable operation of silicon surfaces under variable environmental conditions. The character of the micro-mechanical response at very small deformations (nanometer-scale indentation depths) is especially critical for nanoscale coatings in nano- and micro-electromechanical devices (NEMS and MEMS) [1]. For such devices, the dynamic state of mating surfaces critically depends upon normal and shear stresses developed within a nanometer scale contact area [2–4]. Various versions of protective compliant coatings have been proposed to reduce friction and adhesion between mating microscopic parts made mainly from silicon. Deposition of a molecularly thick organic layer via chemical self-assembly, so called self-assembled monolayers (SAMs), has been proposed and realized recently. Indeed, SAMs have dramatically reduced friction and adhesion and have found use in various MEMS devices [5–8]. However, alkyl chains do not sustain high compression and shear stresses, which significantly limits their useful life [9]. Recently, we have proposed that nanocomposite polymer layers capable of very large elastic deformation can exhibit superior nano- and micro-tribological properties [10,11]. Following this strategy, we fabricated a compliant layer of tri-block copolymer, grafted to a silicon surface using the anchoring properties of an epoxysilane surface [12]. We investigated both the chemical composition and micro-mechanical and tribological properties of the grafted SEBS layer [12–14].

This paper discusses further developments in the fabrication and micro-tribological studies of the nanocomposite coatings composed of a cross-linked polymer layer tethered to a compliant interlayer from a reinforced rubber phase. We report on a new design of this nanoscale coating with a total thickness below 30 nm, which demonstrates a non-linear nano-mechanical response and low friction as reported earlier [15]. The compliant rubber layer is grafted to a silicon surface via anchoring epoxy-silane SAM [16]. The rubber interlayer is covered by the tethered hard layer of a copolymer of methylmethacrylate (MMA) and 1,6-hexanediol dimethacrylate (HDM) as a cross-linker (Fig. 1). We choose the copolymer poly(methylmethacrylate–1,6-hexanediol dimethacrylate) (PMA) because of its high elastic modulus

* Corresponding author. Tel.: +1-515-294-6904; fax: +1-515-294-5444.
*E-mail address:* vladimir@iastate.edu (V.V. Tsukruk).

0043-1648/02/$ – see front matter © 2002 Elsevier Science B.V. All rights reserved.
PII: S0043-1648(02)00048-0

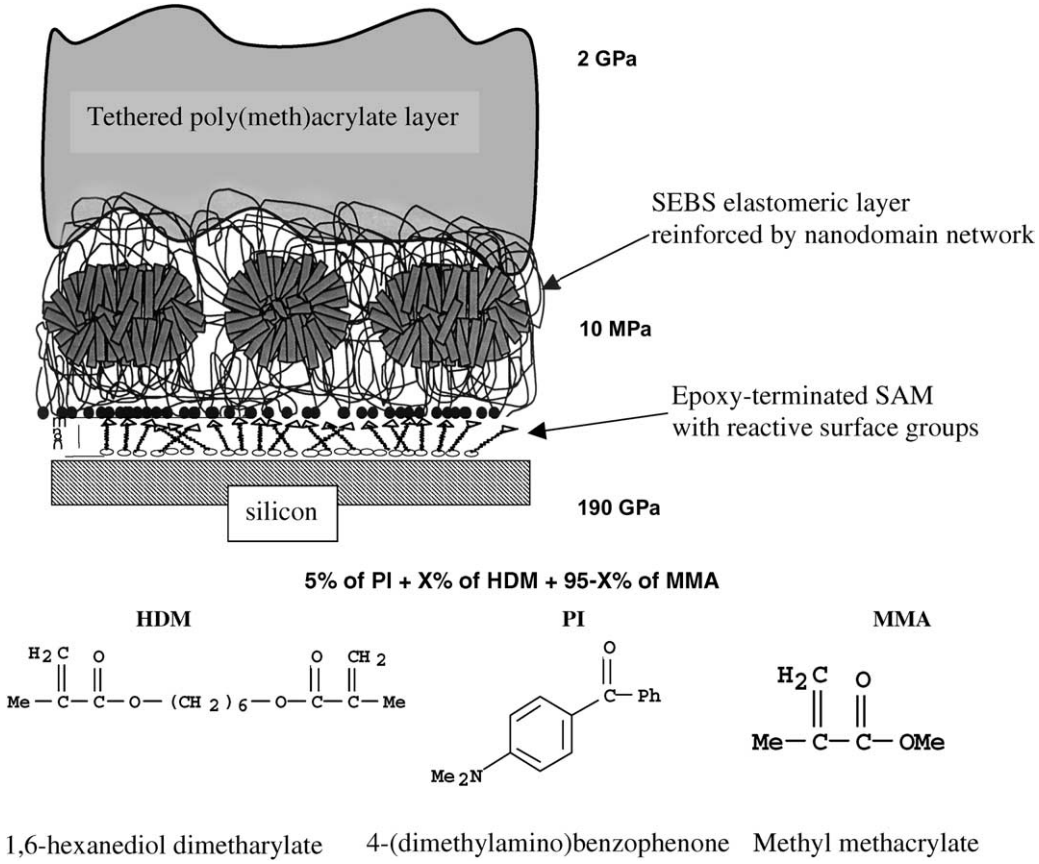


Fig. 1. Architecture of sandwiched trilayer with values of elastic modulus for different layers (top) and chemical formulas of the initial mixture of chemicals for photopolymerization (bottom).

(about 2 GPa) as compared with the rubber layer and micro-heterogeneous morphology, which is instrumental in the formation of grainy polymer layers [17]. We expected to obtain a nano-grainy structure in the crosslinked hard polymer on top of a smooth compliant reinforced rubber layer. Furthermore, we expected to observe peculiar micro-mechanical and -tribological behavior in the "sandwiched" composite. We investigated the effect of chemical composition of the topmost layer on its morphology and on the nano-mechanical and micro-tribology properties of the multilayer coating.

## 2. Experimental

Highly polished single-crystal silicon wafers of {1 0 0} orientation (Semiconductor Processing Co.) were used as substrates. (3-Glycidoxypropyl)trimethoxysilane (Aldrich) was used to prepare epoxy-terminated SAM on the silicon surface [16]. The primary compliant layer was formed from the tri-block copolymer, poly[styrene-b-(ethylene-co-butylene)-b-styrene] (SEBS), (Kraton 1901, Shell) with glassy polystyrene (PS) domains embedded in rubber polyethylenebuthylene (PEB) matrix. This layer was grafted to the epoxy-terminated SAM according to a procedure described in detail earlier [12]. The thickness of the grafted SEBS layer was 8.4 ± 0.4 nm. Both compounds, HDM and photoinitiator 4-(dimethylamino) benzophenone (PI) (Fig. 1) (Aldrich) were used as received. The solution of monomers was deposited directly on to the rubber layer, covered with a glass plate, and exposed to UV light to initialize photopolymerization and the formation of PMA. After polymerization, the glass plate was removed, the sample was rinsed thoroughly with toluene and treated in an ultrasonic bath to remove residual monomer and ungrafted polymer.

The thickness and the microstructure of the polymer layers were determined from ellipsometry, scanning probe microscopy (SPM), scanning electron microscopy (SEM), and Auger spectroscopy (AES). Ellipsometry measurements were performed with a COMPEL automatic ellipsometer (InOmTech Inc.) at an angle of incidence of 70°. Surface imaging was performed using tapping mode with a Dimension 3000 (Digital Instruments Inc.) SPM microscope according to the usual procedure adapted in our laboratory [18,19]. Micro-mechanical measurements and surface micro-mapping were carried out in the contact mode according to the experimental procedure described earlier, which used a so-called force volume mode and a Hertzian

contact mechanics model to evaluate compression modulus depth profile [20,21].

The surface composition distribution and SEM images were obtained with a PHI-670 Auger electron spectrometer. AES surface analysis was performed using a field emission gun with an accelerating voltage of 5 kV and a current of 0.0211 mA. The working potential for depth sputtering was 1 kV using Ar-ions. Under this working condition, the sputtering rate was 0.47 nm/min when calibrated against $SiO_2$.

For micro-tribological measurements, we employed an oscillating friction and wear tester. The 3 mm diameter steel ball with a very smooth surface (surface micro-roughness $<10$ nm within 2 μm × 2 μm) was mounted in a carrier head and oscillated against a stationary layer-deposited planar specimen with applied load of 0.3 and 1.8 N which corresponded to a maximum Hertzian pressure of 660 MPa and 1.2 GPa. Sliding speed was 4.43 mm/s and the stroke length was 3 mm.

## 3. Results and discussion

### *3.1. Microstructure of sandwiched layers*

The microstructure of the topmost PMA layer tethered to the rubber interlayer is as shown in Fig. 2. The PMA layer showed continuous and uniform morphology over large surface area with fine grainy structure resolved at high

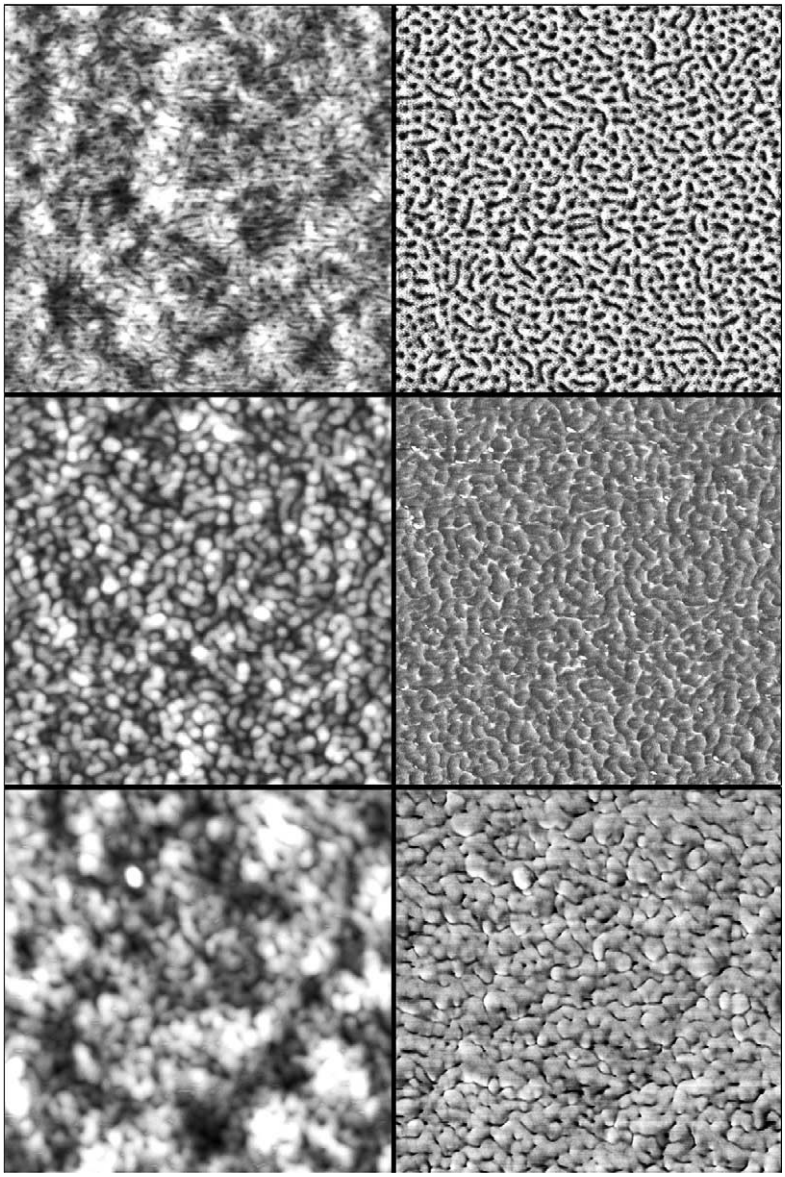

Fig. 2. The AFM images of the rubber SEBS interlayer (top) and sandwiched film containing 3% of HDM (middle) and 15% of HDM (bottom): left is topography; right is phase image. Scan size is 1 μm × 1 μm for all images. Height and phase scales are changed for top to bottom from 5 nm, 15° to 10 nm, 15° and to 20 nm, 60°.

magnification. This grainy structure for the PMS layer was very different from that observed for glassy PS domains distributed in the rubber layer of SEBS polymer (Fig. 2). The polymer grains showed a wide distribution of sizes in the range of 50–100 nm. The morphological characteristics of the PMA layer formed at different stages are as shown in Fig. 3. The micro-roughness of the PMA layer of 4–5 nm was high compared with the rubber interlayer (0.25 nm) (Fig. 3).

The increase of concentration of cross-linker, HDM, in the initial mixture resulted in an increase of the micro-roughness of the PMA layer. The lateral size and height of the surface grains increased with the increase of HDM content beyond 6% in the composition of the PMA layer as shown in Fig. 3. Accordingly, the apparent surface area of grains decreased due to an increasing surface fraction of deeper grooves situated in between grains. Higher concentration of HDM (above 6%) produced larger lateral size of the grains and their aggregation in dense clusters separated by grooves (Fig. 2). As a result, the apparent surface area of grains increased and the surface micro-roughness remained unchanged for these compositions (Fig. 3).

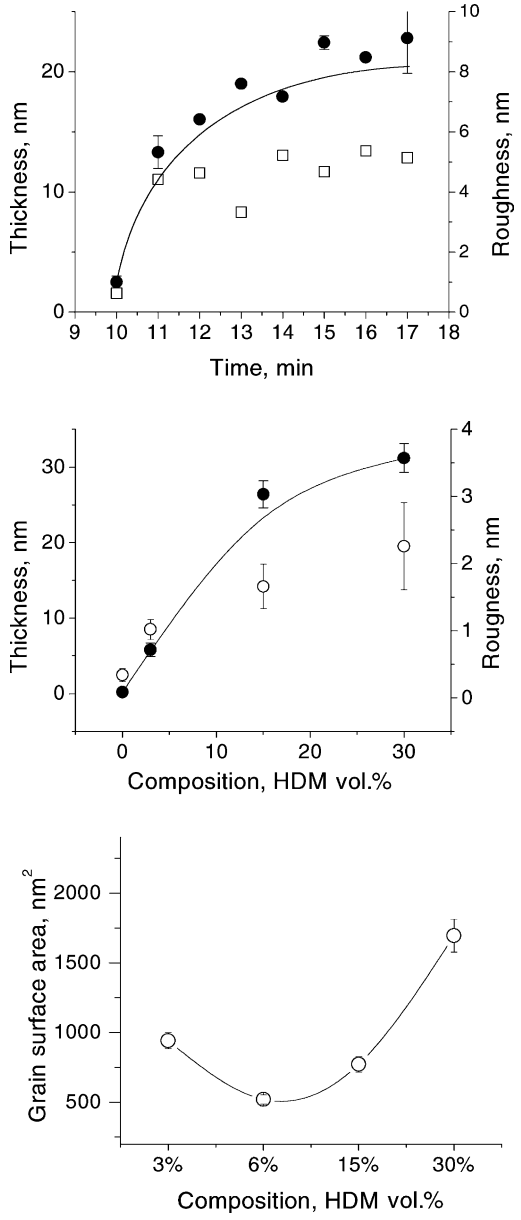


Fig. 3. Thickness and micro-roughness of the PMA layer with 100% of HDM as a function of UV light exposition (top) and for different chemical compositions (percentage of HDM component) at UV light exposure of 20 min (middle): closed circles means thickness (nm) and open boxes/circles means roughness (nm). The average surface grain area for different chemical compositions (HDM (vol.%)) at UV light exposure of 20 min (bottom).

The surface morphology observed and its variation with chemical composition are in agreement with the results of Bowman et al. for photopolymerizable polymers [17]. It has been demonstrated that for lower cross-linking density structural heterogeneity increases with the increase of cross-linking of polymethylmeth acrylate material. The grainy morphology was typical for cross-linked PMA compounds and reflected the micro-heterogeneous microstructure caused by non-uniform photopolymerization initiated in random nuclei, which grew to certain dimensions before interfering with each other. Grains represented initial micro-gel volumes with a high density of cross-linking and the inter-grain space was characterized by lower cross-linking density. Thus, from a micro-mechanical point of view, one can expect that the elastic deformation behavior of this material should involve displacement of hard domains within a more compliant matrix.

After the inhibiting period of 10 min caused by the presence of a stabilizer and oxygen in the initial mixture, the photopolymerization leads to the formation of the complete PMA layer on the top of SEBS interlayer (Fig. 3). The thickness of the layer reached the plateau value after 15–20 min. Under these conditions, the PMA layer showed a well-developed grainy microstructure. We stopped illumination at this stage because further illumination results in the formation of fully cross-linked PMA, which showed a more uniform microstructure. The changes in surface microstructure of the thin polymer layer followed known tendencies for bulk photopolymerization. In fact, the kinetics of photopolymerization of these multifunctional (meth)acrylates was the subject of many investigations [22–24]. Inhibiting period and post-polymerization are characteristics of the micro-heterogeneous photopolymerization of multifunctional (meth)acrylates. Several researchers [24,25] have shown fine grainy microstructure and demonstrated that one of the most fundamental structural characteristics of highly cross-linked network formation was spatial heterogeneity in the polymerizing system and micro-gel formation during cross-linking reactions. Spatial micro-gels are regions of densely crosslinked and cycled polymers in a more loosely cross-linked matrix. This is caused by the enhanced reactivity of functional groups near the active radical site. The relative reactivity of the cross-linking monomers was found to influence the cycle rank, which determined the elastic properties of the network. The nature of the cross-linking

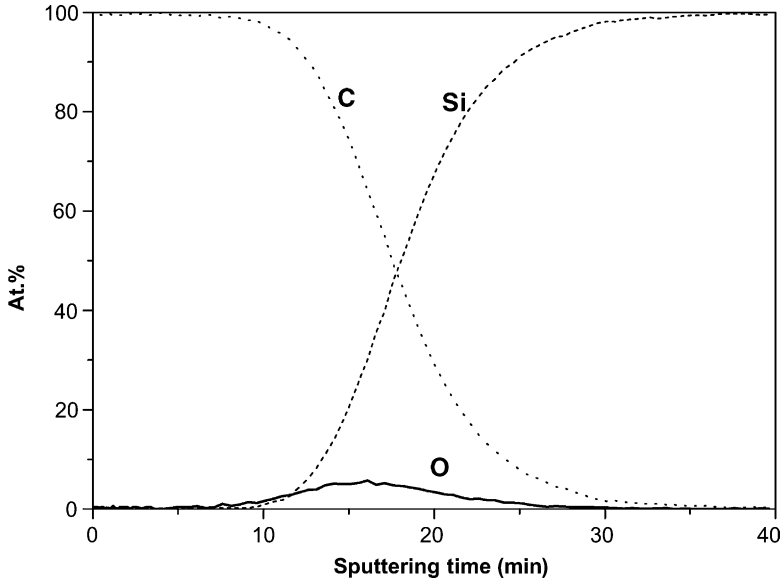


Fig. 4. The depth distribution of chemical composition within the polymer trilayer coating as determined from AES. The sputtering rate was 0.47 nm/min as calibrated against $SiO_2$.

free radical mechanism and the enhanced reactivity of the pendant double bonds in the vicinity of the radical resulted in polymer–polymer aggregation at low conversions (i.e. the formation of micro-gels). The heterogeneity dramatically changes as a function of conversion and polymerization conditions. As the polymerization reaches higher conversions, the polymer micro-gels become more homogeneously distributed.

The nature of the cross-linker played an important role in the formation of the tethered PMA layer. As we observed, a pure PMA composition without HDM was unable to tether to the rubber layer. In contrast, the PMA layer demonstrated perfect stability against multiple washing in both polar (THF) and non-polar (toluene) hot solvents combined with the ultrasonic bath. We suggest that PS domains were swollen with the mixture of MMA and HDM during its deposition on the substrate. During the photopolymerization, a three-dimensional network of the cross-linked PMA domains was formed and partially included the PS nano-domains of the SEBS. Indeed, AES revealed the vertical distribution of elements, which confirmed our suggestions (Fig. 4). AES data showed the strong presence of the carbon in the whole film (30 nm thick), with silicon being a predominant element at greater depth (the depth can be estimated only approximately due to different etching rate for different elements). Oxygen was mainly concentrated in the middle of the film, at the interface between the rubber interlayer and the topmost PMA layer (Fig. 1). This distribution confirmed that significant diffusion of the oxygen-containing component of the initial mixture takes place within the rubber matrix with a very small content of oxygen (predominantly carbon-containing PS and PEB fragments). Obviously, this resulted in the micro-gel network deeply interpenetrating the supporting rubber matrix and providing firm tethering of the topmost layer and the rubber interlayer.

### 3.2. Micro-mechanical properties

The micro-mechanical properties of individual components of the "sandwiched" coatings were measured as follows. As a reference sample, we prepared a layer of PMMA spin-coated on a bare silicon wafer with a thickness of about 50 nm. The elastic modulus of the model PMMA layer was found to be about 2.5 GPa, which is close to the value from macroscopic mechanical measurements [17] and is typical for flexible polymer networks [26]. The rubber interlayer was highly compliant with an elastic modulus of 10 MPa as reported earlier [27]. Finally, the silicon substrate itself was very hard with the elastic modulus of 190 GPa. We neglected the effect of the epoxysilane SAM because it was very thin (about 0.7 nm).

Fig. 5 displays the surface morphology and micro-mapping of the sandwiched coating with a hole intentionally produced (during top glass pulling-off) in the center of the images. This hole penetrated the 14 nm topmost PMA layer down to the rubber interlayer, as can be seen from the cross-sectional analysis of the surface topography presented in Fig. 5e. Micro-mapping testing of the surface nano-mechanical response was performed with a pixel-by-pixel nano-indentation of the film, as described earlier [21]. Indentation depth was kept within the range of 2–20 nm to avoid surface instabilities during initial tip engagement and an excessive contribution from the stiff silicon substrate. These conditions for nano-probing provided spatial resolution of 0.2 nm in the vertical direction and 20–50 nm within the $x$ and $y$ planes.

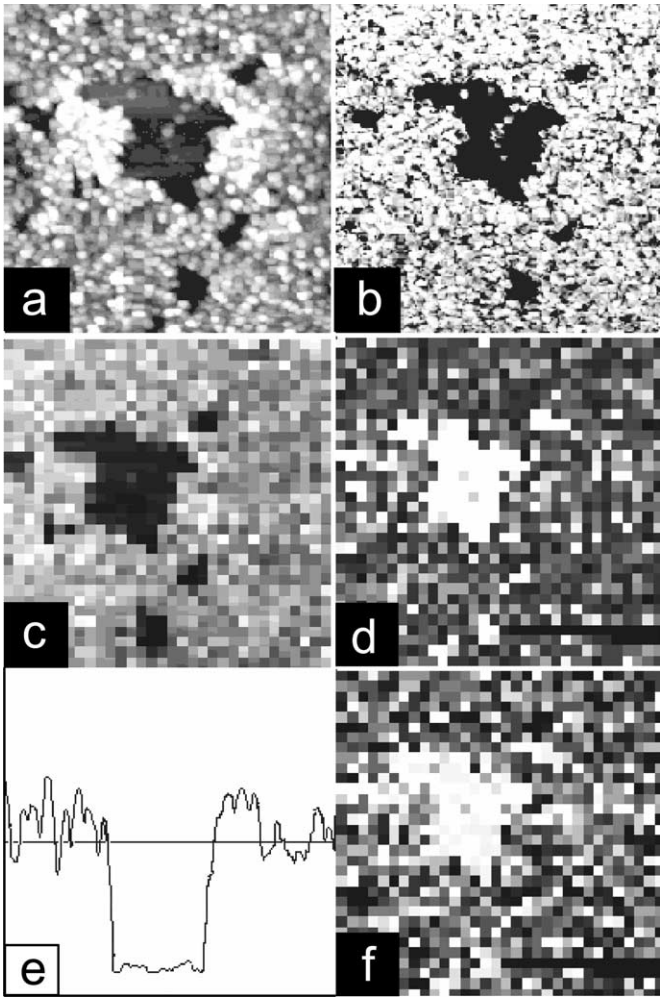


Fig. 5. (a) The AFM topographical and (b) phase of the film surface with a central hole produced during pull-off test, 3 μm × 3 μm surface area with clearly visible grainy microstructure. Micro-mapping of surface properties of the film with 32 pixel × 32 pixel resolution within the same surface area: (c) topography, (d) elastic modulus, and (f) adhesive forces; (e) cross-section of the center of the topographical image, which shows the thickness of the topmost layer of 14 nm that corresponds to the value obtained from independent ellipsometry measurements.

The surface distribution of both the adhesive force and the elastic response showed a clear correlation with surface topography, in that the highest adhesion and elastic modulus were observed within the hole (Fig. 5). Higher adhesion of the rubber interlayer was a result of its higher compliance, which led to a larger contact area at the pull-off point. Higher "apparent" elastic modulus within the hole was caused by the proximity of the underlying silicon substrate. The high resolution imaging of the surface (not shown) inside the hole demonstrated a morphology identical to the original reinforced rubber layer. Hence, we conclude that the deposition and photopolymerization of the PMA layer did not significantly disturb the nano-domain structure of the rubber interlayer.

We collected force–distance data for the initial rubber layer freely deposited on silicon and the rubber interlayer in the hole after the topmost layer removal. The modulus value was obtained from these data as a function of a penetration depth by using the Hertzian model of the elastic contact combined with a double-spring model with variable spring constants [21]. Both the original rubber layer and the rubber interlayer in the hole demonstrated a constant value of modulus for low penetration (modest compressions) followed by a sharp increase near the stiff silicon surface (Fig. 6). However, the rubber interlayer under the topmost layer showed much higher (three times) apparent elastic modulus as compared with a free surface of the rubber layer. This difference can be related to the additional entanglements and cross-linkings introduced by the photopolymerization of the reactive mixture penetrating into the interlayer as suggested above. It is worth noting that non-linear modulus depth profiles for the sandwiched coatings were similar to the variation of surface hardness reported for a nanocomposite layer from gold layer deposited on top of a compliant dendritic layer [28].

In the course of micro-mapping of various surface areas, we found that the elastic response varied significantly

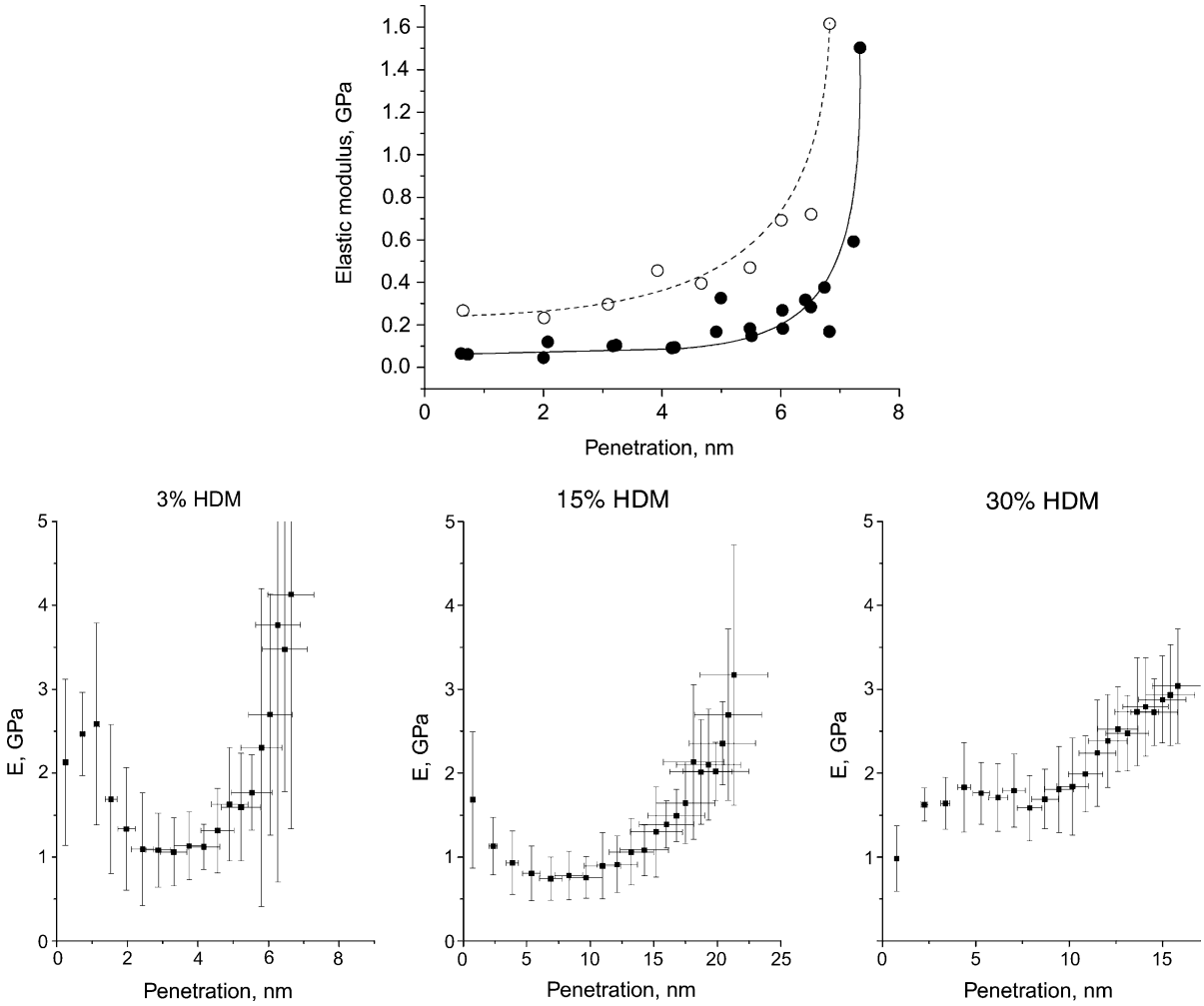


Fig. 6. (Top) a depth profile of the elastic modulus evaluated from force–distance data for the rubber layer grafted to silicon (filled circles) and for the rubber interlayer probed within the hole made by pull-off test (open circles). The thickness of both layers was about 8.5 nm in both cases. (Bottom) a depth profile of the elastic modulus evaluated for the sandwiched coatings with for a different chemical content of the topmost PMA layer: 3 vol.% of HDM (left); 15 vol.% of HDM (middle); and 30 vol.% of HDM (right). Error bars show variations at different surface areas.

depending upon the precise location of the SPM tip (on top of the grains or in-between). The result of the evaluation of the depth variation of the elastic modulus are presented in Fig. 6 as the averaged elasticity profiles collected from 15–20 independent locations. The samples with 3 and 15% of the HDM component demonstrated clear non-linear mechanical response with higher initial modulus for indentation depth below 2 nm, followed by lower modulus at intermediate depths, and much higher values in proximity to the stiff silicon substrate. For indentation depths below 1 nm, the elastic modulus was about 2 GPa, which was close to the expected value for the PMA layer itself. The sample with a high ratio of the cross-linker (30%) demonstrated more monotonic nano-mechanical response because high cross-linking density resulted in more uniform layered microstructure. This demonstrates the critical importance of well-developed grainy microstructure for polymer layers with intermediate cross-linking density in the realization of their non-linear nano-mechanical response, reflecting overall sandwiched architecture of the coatings.

### 3.3. Friction and wear stability

Micro-mechanical probing demonstrated that the special trilayer architecture of the polymer coatings causes their very peculiar non-linear elastic deformational behavior. We believe that the rubber interlayer positioned between the stiff substrate and the topmost polymer layer absorbs the normal deformation stresses and dissipates the mechanical energy during compression. The mechanical stability of the “sandwiched” films under shear stresses is a critical issue for the application of these coatings for mechanically loaded, mating surfaces. Therefore, ultimately, we performed friction and wear resistance measurements on sandwiched coatings.

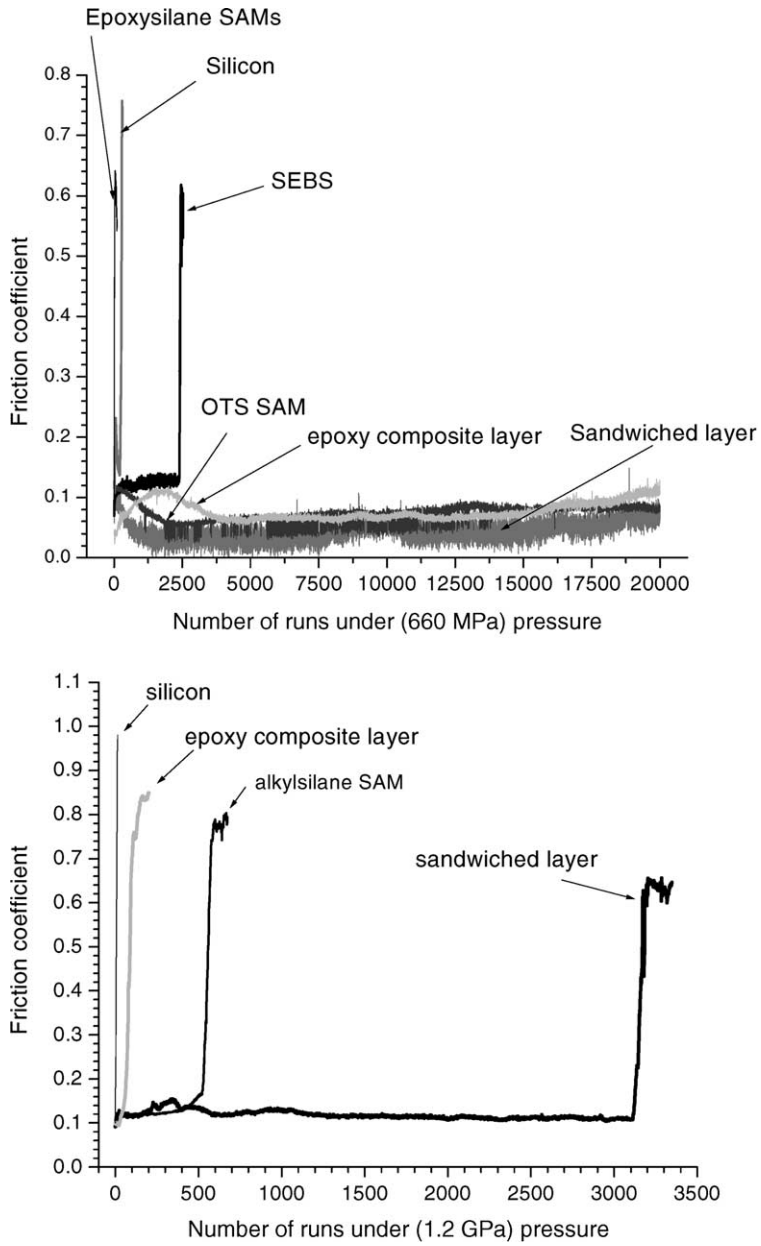


Fig. 7. A value of friction coefficient against a steel ball vs. a number of reciprocal sliding runs for different surface layers at low (top) and high (bottom) normal loads.

The variation of the coefficient of friction against the sliding steel ball as a function of a number of sliding cycles is shown for the sandwiched film with a thickness of the topmost layer of 22.8 nm in comparison with bare silicon surface, epoxy-composite layer of 15 nm fabricated and described earlier [29] and alkylsilane SAM (octadecyltrimethoxysilane, OTS, $C_{16}$), which is a common molecular lubricant for silicon surfaces (Fig. 7) [7]. At the low load of 0.3 N, which corresponded to local maximum pressure of 660 MPa and a radius of the contact area of about 14 μm, both the sandwiched coating and SAM layer showed very comparable micro-tribological performance. They, as well as the epoxy-composite films discussed earlier [29], showed unchanged response and were stable up to 20,000 sliding cycles (the highest number of cycles tested in this work). At the end of this test, the polymer coating showed a modest wear track as shown in Fig. 8. The amount of carbon decreased in the partially worn areas and traces of the underlying silicon showed up in AES spectrum (Fig. 8). On this spectrum, the oxygen band became intense, showing that oxidation of the polymer layer under local mechanical stresses and temperature was a predominant mechanism of gradual deterioration during repeated runs of the steel ball. The value of friction coefficient was within 0.05–0.08 for the SAM layer and reached 0.11 for the epoxy-composite film. The friction coefficient was significantly lower for the sandwiched layer,

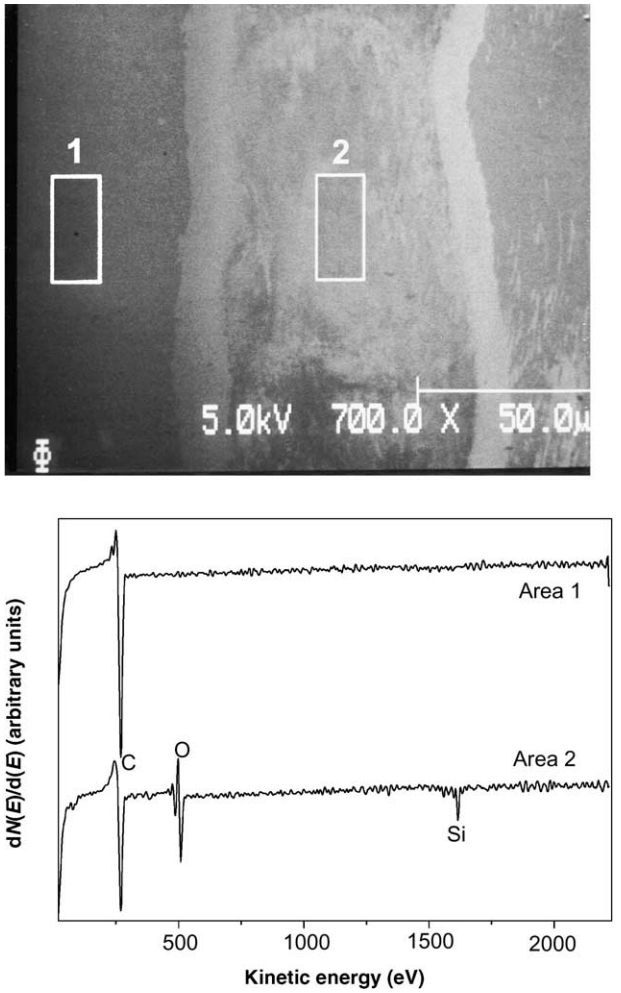


Fig. 8. The SEM image of the wear track for a partially worn surface of a silicon wafer coated with the sandwiched layer (top). Rectangles indicate surface areas (intact and affected) used for AES analysis (bottom plot shows different labeled elements).

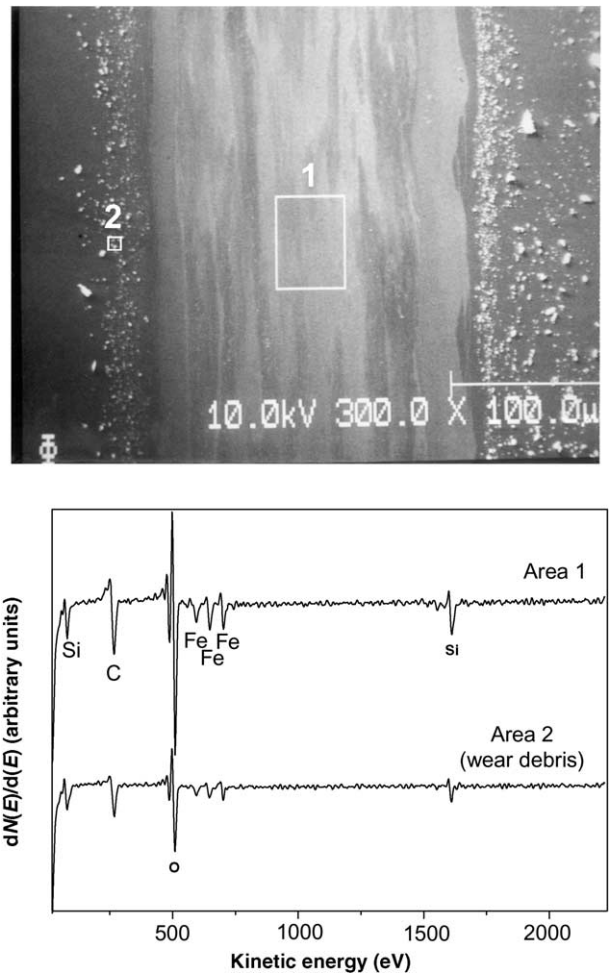


Fig. 9. The SEM image of the wear track for a completely worn surface of a silicon wafer coated with the sandwiched layer after final failure. Rectangles indicate surface areas (intact and wear debris) used for AES analysis (bottom plot shows different labeled elements).

not exceeding 0.06 even for the highest number of cycles tested. Finally, the reference silicon substrate without any organic coating failed within 200 cycles after test initiation (here and later all data were averaged over three independent measurements at various surface locations).

When the local pressure increased, the bare silicon failed almost immediately, followed by a complete failure of the epoxy-composite coating after only 200 sliding cycles (Fig. 7). The SAM layer failed after 900 cycles and, finally, the sandwiched coating was worn down after 3300 cycles. A sharp increase in friction force indicated direct contact and seizure between the mating hard surfaces (steel–silicon). The worn area displayed a well-defined track surrounded by multiple debris that indicates a plowing mechanism of wear at the final stage (Fig. 9) [30]. AES data showed the significant presence of iron and iron oxide in worn areas as well as in the surrounding debris (Fig. 9), which confirmed severe damage of both the silicon substrate and the steel ball.

## 4. Conclusions

We demonstrated that a polymer trilayer film with a nanoscale thickness of 20–30 nm can be designed to serve as a wear resistant protective nanoscale coating for silicon surfaces. This surface structure is formed by a multiple grafting technique involving chemical grafting of SAM and functionalized tri-block copolymer, followed by the photopolymerization of the topmost polymer layer. The unique design of this coating includes a sandwiched, triplex structure with a compliant rubber interlayer mediating local stresses transferred through the topmost hard layer. This architecture provides non-linear mechanical response under compression stresses and allows additional dissipation of mechanical energy via the reversibly compressed rubber interlayer. At modest loads, this coating showed a lower friction coefficient than a classic molecular lubricant, alkylsilane SAM. At the highest pressure tested in this work, 1.2 GPa,

and at the relatively high sliding velocity of 4.4 mm/s, the sandwiched coating designed here were four times more wear resistant than the SAM coating. The predominant wear mechanism was stress and temperature-induced oxidation in the contact area followed by severe plowing wear.

## Acknowledgements

We acknowledge useful discussions with Drs. V.V. Gorbunov and I. Luzinov. This work is supported by The National Science Foundation, Surface Engineering and Solid Mechanics Program, Grant CMS-0099868 and the National Research Laboratory Program of the Korean Ministry of Science and Technology.

## References

[1] H.G. Graighead, Nano-electromechanical systems, Science 290 (2000) 1532.
[2] R.S. Muller, Micro-dynamical systems, in: B. Bhushan (Ed.), Micro-/Nano-Tribology and its Applications, Kluwer Academic Publishers, Dordrecht, 1997, pp. 579–599.
[3] C.M. Mate, J. Wu, Nano-tribology of polymer surface for disk drive applications. in: V.V. Tsukruk, K. Wahl (Eds.), Microstructure and Microtribology of Polymer Surfaces. Proceedings of the ACS Symposium Series, Vol. 741, 2000, pp. 405–417.
[4] B. Bhushan (Ed.), Tribology Issues and Opportunities in MEMS, Kluwer Academic Publishers, Dordrecht, 1998.
[5] V. DePalma, N. Tillman, Friction and wear of self-assembled trichlorosilane monolayer films on silicon, Langmuir 5 (1989) 868.
[6] K. Komvopoulos, Surface engineering and micro-tribology for micro-electromechanical systems, Wear 200 (1996) 305.
[7] M.R. Houston, R.T. Howe, R. Maboudian, Effect of hydrogen termination on the work of adhesion between rough polycrystalline silicon surfaces, J. Appl. Phys. 81 (1997) 3474.
[8] M.T. Dugger, D.C. Senft, G.C. Nelson, Friction and durability of chemisorbed organic lubricants for micro-electromechanical system, in: V.V. Tsukruk, K. Wahl (Eds.), Microstructure and Microtribology of Polymer Surfaces. Proceedings of the ACS Symposium Series, Vol. 741, 2000, pp. 455–473.
[9] J.N. Israelachvili, Intermolecular and Surface Forces, 2nd Edition, Academic Press, New York, 1992.
[10] V.N. Bliznyuk, M.P. Everson, V.V. Tsukruk, Nano-tribological properties of organic boundary lubricants: Langmuir films versus self-assembled monolayers, J. Tribol. 120 (1998) 489.
[11] V.V. Tsukruk, Nanocomposite polymer layers for molecular tribology, Tribol. Lett. 10 (2001) 127.
[12] I. Luzinov, et al., Thermoplastic elastomeric monolayers grafted to silicon surfaces, Macromolecules 33 (2000) 7629.
[13] I. Luzinov, et al., Nano-tribological behavior of tethered reinforced polymer monolayers, Tribol. Int. 34 (2001) 327.
[14] I. Luzinov, et al., Stability of micro-domain morphology in tethered block-polymer monolayers, Polymer 42 (2001) 2267.
[15] V.V. Tsukruk, A. Sidorenko, H. Yang, Multilayered nano-coatings with non-linear elastic response, Polymer 43 (2002) 1695.
[16] V.V. Tsukruk, I. Luzinov, D. Julthongpiput, Epoxy-terminated self-assembled monolayers: molecular glues for polymer layers, Langmuir 15 (1999) 3029.
[17] Anand Kumar, R. Kannurpati, Use of living radical polymerizations to study the structural evolution and properties of highly crosslinked polymer networks, J. Polym. Sci.: Part B. Polym. Phys. 35 (1997) 2297.
[18] V.V. Tsukruk, Scanning probe microscopy of polymer surfaces, Rubber Chem. Technol. 70 (30) (1997) 430.
[19] V.V. Tsukruk, D.H. Reneker, Scanning probe microscopy of polymeric and organic molecular films: from self-assembled monolayers to composite multilayers, Polymer 36 (1995) 1791.
[20] V.V. Tsukruk, V.V. Gorbunov, Nano-mechanical probing with scanning force microscopy, Microsc. Today 1 (2001) 8.
[21] V.V. Tsukruk, Z. Huang, Micro-thermomechanical properties of heterogeneous polymer films, Polymer 41 (2000) 5541.
[22] A.R. Kannurpati, et al., A study of the evolution of mechanical properties and structural heterogeneity of polymer networks formed by photopolymerizations of multifunctional (meth)acrylates, Polymer 39 (12) (1998) 2507.
[23] A.R. Kannurpati, C.N. Bowman, Structural evolution of dimethacrylate networks studied by dielectric spectroscopy, Macromolecules 31 (1998) 3311.
[24] T. Scherzer, U. Decker, The effect of temperature on the kinetics of diacrylate photopolymerizations studied by real-time FT-IR spectroscopy, Polymer 41 (2000) 7681.
[25] K.S. Anseth, C.N. Bowman, Kinetic gelation predictions of species aggregation in tetrafunctional monomer polymerizations, J. Polym. Sci.: Part B. Polym. Phys. 33 (1995) 1769.
[26] V. Krevelen DW, Properties of Polymers, Elsevier, Amsterdam, 1997.
[27] V.V. Tsukruk, A. Sidorenko, V.V. Gorbunov, S.A. Chizhik, Surface nano-mechanical properties of polymer monolayers with domain structure, Langmuir 17 (2001) 6715.
[28] S.C. Street, et al., Unique structural and mechanical properties of ultrathin au films grown on dendrimer-mediated substrates, Chem. Mater. 13 (2001) 3669.
[29] I. Luzinov, D. Julthongpiput, P.D. Bloom, V.V. Sheares, V.V. Tsukruk, Bilayer nanocomposite molecular coatings from elastomeric/rigid polymers: fabrication, morphology, and micro-mechanical properties, Macromol. Symp. 167 (2001) 229.
[30] E. Rabinowicz, Friction and Wear of Materials, Wiley, New York, 1965.